

Architecture-Aware Minimization (A²M): How to Find Flat Minima in Neural Architecture Search

Matteo Gambella, Fabrizio Pittorino, Manuel Roveri
Department of Electronics, Information and Bioengineering, Politecnico di Milano
Via Ponzio 34/5, Milano, 20133, Italy
{matteo.gambella, fabrizio.pittorino, manuel.roveri}@polimi.it

March 14, 2025

Abstract

Neural Architecture Search (NAS) has become an essential tool for designing effective and efficient neural networks. In this paper, we investigate the geometric properties of neural architecture spaces commonly used in differentiable NAS methods, specifically NAS-Bench-201 and DARTS. By defining flatness metrics such as neighborhoods and loss barriers along paths in architecture space, we reveal locality and flatness characteristics analogous to the well-known properties of neural network loss landscapes in weight space. In particular, we find that highly accurate architectures cluster together in flat regions, while suboptimal architectures remain isolated, unveiling the detailed geometrical structure of the architecture search landscape. Building on these insights, we propose Architecture-Aware Minimization (A²M), a novel analytically derived algorithmic framework that *explicitly* biases, for the first time, the gradient of differentiable NAS methods towards flat minima *in architecture space*. A²M consistently improves generalization over state-of-the-art DARTS-based algorithms on benchmark datasets including CIFAR-10, CIFAR-100, and ImageNet16-120, across both NAS-Bench-201 and DARTS search spaces. Notably, A²M is able to increase the test accuracy, on average across different differentiable NAS methods, by +3.60% on CIFAR-10, +4.60% on CIFAR-100, and +3.64% on ImageNet16-120, demonstrating its superior effectiveness in practice. A²M can be easily integrated into existing differentiable NAS frameworks, offering a versatile tool for future research and applications in automated machine learning. We open-source our code at <https://github.com/AI-Tech-Research-Lab/AsquaredM>.

1 Introduction

Neural Architecture Search (NAS) has emerged as a powerful paradigm in machine learning, offering the potential to automatically identify optimal neural network (NN) architectures for a given task [1]. In recent years, NAS has gained broad attention due to its versatility and applicability in scenarios where computational or hardware constraints demand efficient and specialized models, such as mobile devices or edge computing environments [2, 3]. Fundamentally, NAS can be framed as a discrete optimization process over a vast space of neural architectures. Early approaches relied on methods like genetic algorithms [4] and reinforcement learning [5]. However, the high computational cost associated with these methods motivated the development of more efficient strategies, resulting in the introduction of differentiable relaxations of the problem, such as Differentiable Architecture Search (DARTS) [6] and its numerous variants [7, 8, 9, 10, 11, 12, 13], which offer a more tractable way to navigate large architecture spaces. These methods were also promising in terms of performance, making them increasingly popular in the field.

While considerable research efforts have been devoted to understanding the geometry of neural network loss landscapes in weight space [14, 15, 16, 17, 18], the precise geometry of architecture spaces remains largely underexplored [19, 20]. A deeper understanding of architecture geometry is crucial for designing more effective NAS algorithms, and for gaining insights into both the nature of the neural architecture optimization problem and the fundamental question of *why certain architectures generalize better than others*.

In this work, we shed light on these questions by focusing on two representative differentiable NAS search spaces: the NAS-Bench-201 benchmark dataset [21] and the DARTS search space [6]. Our

investigation aims to uncover and quantify the geometrical properties of these neural architecture spaces. We introduce new procedures to explore neighborhoods and loss paths in these spaces, allowing us to systematically examine how performance changes as we traverse from one architecture to another, possibly distant, one. Our analysis reveals that *high-accuracy architectures tend to cluster in flat regions of the architecture space, whereas less accurate architectures appear in more isolated regions*. This behavior suggests the existence of *basins of good architectures* analogous to the flat minima observed in weight space optimization [22, 23, 24, 25].

Building on these observations, we introduce Architecture-Aware Minimization (A²M), an algorithmic approach that redefines the bi-level optimization process in DARTS. The novel contribution of A²M resides in its ability to reformulate the gradient update on the *architecture* space, leveraging the geometric insights we have uncovered to successfully bias the search process towards flat regions in the architecture space, analytically extending to the architecture space the concept of Sharpness-Aware Minimization (SAM) [26] in weight space. This shift from optimizing flatness in weight space to optimizing it in architecture space enhances generalization beyond existing DARTS-based methods by explicitly shaping the optimization process in the architecture landscape for greater robustness with respect to architectural perturbations. We demonstrate the effectiveness of A²M across multiple benchmarks, including CIFAR-10, CIFAR-100, and ImageNet16-120, on both NAS-Bench-201 and DARTS search spaces. In particular, A²M increases test accuracy by +3.60% on CIFAR-10, +4.60% on CIFAR-100%, and +3.64% on ImageNet16-120, on average over several state-of-the-art (SotA) DARTS methods, and can be easily integrated with differentiable NAS procedures.

Our novel contributions are summarized as follows:

1. Through the definition of distance in architecture space, we (i) introduce the notion of architecture neighborhoods at a given radius to unveil clusters of high-performing architectures, and (ii) we are able to construct paths between architectures at a given distance, providing deeper insights into architecture loss-landscapes and its design properties.
2. We derive a new, analytically grounded update rule for the architecture parameters in DARTS, providing the basis for our Architecture-Aware Minimization (A²M) algorithm explicitly targeting *flat regions in architecture space*.
3. By easily plugging this new update rule into existing DARTS-based frameworks, we achieve substantial generalization improvements in the final networks across several SotA DARTS-based methods, as demonstrated by our empirical results.

The remainder of the paper is organized as follows. In Section 2, we review related literature on flatness concepts in NAS. Section 3 provides background on the bi-level optimization procedure of DARTS methods and on the SAM gradient step. Section 4.1 presents the construction of neighborhoods and (shortest) paths for exploring the geometry of neural architecture spaces. In Section 5, we introduce the A²M algorithm and offer detailed experimental results comparing it with other SotA DARTS-based methods, showing the superior performances of our method. Finally, Section 6 concludes the paper and outlines future research directions for integrating principled architecture loss landscape exploration in the NAS algorithmic design.

2 Related literature

Many recent variants of Differentiable Architecture Search (DARTS) have focused on mitigating the so-called performance collapse or discretization gap, which arises when the supernet validation performance deviates substantially from the one of the final discrete architecture. A common cause is the supernet’s tendency to overfit by relying heavily on skip connections. Several methods constrain or balance skip connections to address this issue. DARTS– [10] adds auxiliary skip connections between nodes to ensure more uniform contributions from candidate operations. FairDARTS [27] imposes a fairness constraint to penalize dominance by any single operation, while β -DARTS [11] employs a bilevel optimization with an improved regularization term on the architecture parameters, subsequently refined by β -DARTS++ [12] for greater stability and efficiency. Other approaches, among others, include DARTS+ [28], which terminates the search early to prevent overfitting, PC-DARTS [29], which lowers memory use by sampling a subset of channels for each operation during the search, thus reducing bias toward skip connections, and Λ -DARTS [30], which introduces two new loss regularization terms

that aim to prevent performance collapse by harmonizing operation selection via aligning gradients of layers. DARTS-PT [9] instead re-examines how architectures are selected at the end of the search, where architecture parameters are chosen using the *argmax* operator, and proposes a perturbation-based architecture selection scheme to measure each operation’s influence on the supernet, along with progressive tuning.

A complementary body of work tackles the discretization gap through the use of regularization strategies with the aim of enhancing architectural flatness, mainly investigating the properties of the continuous relaxation of the architecture space instead of the true, discrete one. We provide a comprehensive picture of the discrete architecture space, together with a principled and explicit way to bias the search process towards flat regions in this space. Robust DARTS (R-DARTS) [7] is among the first works addressing the instability issues in DARTS. This contribution highlights the role of the Hessian of the validation loss in DARTS, observing that smaller dominant eigenvalues correlate with improved stability and generalization and introducing improved regularization strategies to promote smoother loss surfaces in the search process. Shu et al. [31] visualize the DARTS loss surface by relying on continuous architecture parameters, and show that it can converge to sharp minima, leading to poor generalization. Therefore, they stress the importance of finding new methods to promote flatter regions in architectural space. Other studies have indirectly or empirically approached the flatness problem without relying on principled or explicit flatness optimization. Improvements on the original DARTS method have been observed through its combination with techniques such as self-distillation [13], which improves generalization by transferring knowledge from teacher to student supernets, or the injection of noise into architecture parameters in Chen et al. [8], that propose indirect ways of promoting flatness in DARTS, such as SDARTS (with two variants: random smoothing (SDARTS-RS) and adversarial perturbations (SDARTS-ADV)). NA-DARTS [19] modifies architecture connections (e.g., replacing a convolutional layer with a skip connection) to define a notion of proximity between architecture configurations, and aims to optimize the flatness around them by employing an objective function focused on performance across neighboring configurations. However, this algorithm is not able to obtain significant improvements in model performance. Recent findings [20] indicate that greedy local search methods such as iteratively modifying top-performing architectures in small steps can be effective in finding high-accuracy architectures if the search is started in smooth loss basins.

Our work extends these ideas by providing new tools to visualize and quantify the geometry of NAS search spaces, including the definition of neighborhoods and distance in (discrete) neural architecture spaces, the introduction of paths in the loss landscape between distant architectures, and the distribution of accuracies for neighboring configurations at a certain distance (radius). A comprehensive evaluation on the Nas-Bench-201 and DARTS search spaces is conducted. We then introduce A²M, a novel class of algorithms that analytically introduces the Sharpness-Aware Minimization (SAM) [26, 32] update step directly into the gradient of architecture parameters, *explicitly optimizing flatness in the architecture space for the first time*. Our algorithm can be easily used in conjunction with most differentiable NAS algorithms, generally improves their performance, and offers a unified perspective on how geometric properties of the *architecture space* can be leveraged to achieve robust optimization and improved generalization in neural architecture search.

3 Background

This section provides an overview of two widely studied differentiable NAS search spaces, i.e. DARTS [6] and NAS-Bench-201 [21], followed by a brief review of Sharpness-Aware Minimization (SAM) [26] and its variant USAM [32]. These concepts underlie the A²M algorithm presented in Eq. (8) and derived in Appendix A.

3.1 DARTS Search Space

DARTS is a cell-based NAS framework designed to reduce search dimensionality by concentrating on cell-level structures rather than entire models [6]. Each cell is represented as a directed acyclic graph with nodes with N nodes arranged sequentially and edges connecting them, where operations on each edge are drawn from a shared set of possible operations. Let $\mathcal{O} = \{o^{(i,j)}\}$ be the set of candidate operations between the i -th and j -th nodes. DARTS assigns continuous architecture parameters $\alpha = \{\alpha^{(i,j)}\}$, where each $\alpha^{(i,j)} \in \mathbb{R}^{|\mathcal{O}|}$ weights the choice of operation α on a given edge in a weighted

sum of operations, and must be optimized. The mixed operation is defined as

$$\bar{o}^{(i,j)}(x) = \sum_{o \in \mathcal{O}} \frac{\exp(\alpha_o^{(i,j)})}{\sum_{o' \in \mathcal{O}} \exp(\alpha_{o'}^{(i,j)})} o(x), \quad (1)$$

where the weights are normalized via a softmax function and the network ultimately selects discrete operations via an *argmax* over $\alpha^{(i,j)}$. The output of a cell is computed by applying a reduction operation, such as concatenation, to all intermediate nodes. Each intermediate node is computed based on its predecessors using the *mixed operation* Eq. 1.

The search objective in DARTS is commonly posed as a bi-level optimization:

$$\begin{aligned} \min_{\alpha} F(\alpha) &= \mathcal{L}_{\text{val}}(\mathbf{w}^*(\alpha), \alpha), \\ \text{s.t. } \mathbf{w}^*(\alpha) &= \arg \min_{\mathbf{w}} \mathcal{L}_{\text{train}}(\mathbf{w}, \alpha), \end{aligned} \quad (2)$$

where $\mathcal{L}_{\text{train}}$ and \mathcal{L}_{val} denote the training and validation losses, respectively. The parameter set \mathbf{w} is optimized at the lower level, while the architecture parameters α are optimized at the upper level¹. Differentiating $F(\alpha)$ requires the implicit function theorem [33]:

$$\nabla_{\alpha} F(\alpha) = \nabla_{\alpha} \mathcal{L}_{\text{val}}(\mathbf{w}^*, \alpha) + (\nabla_{\alpha}^{\top} \mathbf{w}^*(\alpha)) \nabla_{\mathbf{w}} \mathcal{L}_{\text{val}}(\mathbf{w}^*(\alpha), \alpha), \quad (3)$$

where

$$\nabla_{\alpha} \mathbf{w}^*(\alpha) = - \left[\nabla_{\mathbf{w}\mathbf{w}}^2 \mathcal{L}_{\text{train}}(\mathbf{w}^*, \alpha) \right]^{-1} \nabla_{\alpha\mathbf{w}}^2 \mathcal{L}_{\text{train}}(\mathbf{w}^*, \alpha). \quad (4)$$

In practice, DARTS applies this formulation to two types of cells: *normal cells*, which preserve spatial dimensions (height and width), and *reduction cells*, which reduce them and increase feature depth. Each cell contains 4 intermediate nodes connected by 14 edges, with 8 candidate operations (including a *zero* operation referring to a missing link between two nodes) on each edge [6]. The graph includes two input nodes and one output node. In convolutional cells, the input nodes are the outputs of the previous two cells. After searching, the final, discrete architecture is constructed by retaining the strongest k operations (from distinct nodes) among all non-zero candidates for each intermediate node.

3.2 NAS-Bench-201

NAS-Bench-201 [21] is an influential benchmark designed to facilitate analysis and comparison across NAS methods. It provides a DARTS-like search space with only normal cells consisting of 4 internal nodes and 5 possible operations per edge, resulting in 15,625 unique architectures. The output of a cell is the output of the last internal node. Each architecture’s performance is tabulated for CIFAR-10 [34], CIFAR-100 [34], and ImageNet16-120 [35], allowing researchers to query final accuracies without retraining from scratch.

3.3 Sharpness-aware Minimization in Weight Space

Sharpness-Aware Minimization (SAM) [26] modifies the standard stochastic gradient descent (SGD) update by encouraging convergence to flatter minima. Let x_k be the parameters on which the gradient is calculated. Then the standard SGD and SAM updates can be written as

$$\text{SGD: } x_{k+1} = x_k - \eta \nabla f(x_k), \quad (5)$$

$$\text{SAM: } x_{k+1} = x_k - \eta \nabla f\left(x_k + \rho \frac{\nabla f(x_k)}{\|\nabla f(x_k)\|^2}\right). \quad (6)$$

USAM [32], an unnormalized variant of SAM, replaces the normalized gradient perturbation with $\rho \nabla f(x_k)$, yielding

$$\text{USAM: } x_{k+1} = x_k - \eta \nabla f\left(x_k + \rho \nabla f(x_k)\right). \quad (7)$$

These updates explicitly encourage solutions that remain stable under small perturbations in parameter space, targeting optimized flatness in the NN loss landscape. Appendix A details how we analytically introduce USAM Eq. (7) into the DARTS bi-level framework Eqs. (3) and (4) to derive the A²M approximated gradient presented in Eq. (8).

¹The final discrete architecture is derived by applying an *argmax* operation to $\{\alpha^{(i,j)}\}$.

4 Flatness Metrics and Algorithms in NAS

In this section, we introduce neighborhoods and paths in discrete NAS spaces to quantitatively investigate their geometry and flatness properties. Inspired by this investigation, we proceed to propose A²M, a new differentiable NAS gradient update step that is easily deployable on top of most DARTS-based methods and improves their performances.

4.1 NAS Space Geometry

To investigate the architecture accuracy landscape of discrete NAS spaces, we introduce methods to analyze its key geometrical properties. Our evaluation examines accuracy distributions at different distances from a reference architecture, local and global geometrical properties, and the impact of architecture modifications on model performance. By analyzing accuracy distributions across different regions of the search space, we identify clustering patterns and flatness properties that influence the robustness and generalization ability of architectures. These insights contribute to a deeper understanding of the structural properties of NAS spaces, informing the design of A²M, our proposed optimization algorithm effectively targeting flat regions.

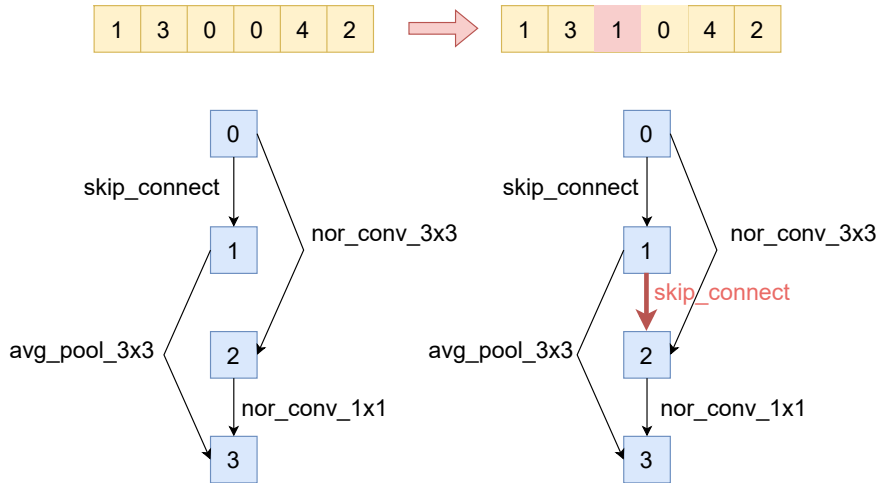


Figure 1: Example of a NAS-Bench-201 architecture and its radius-1 neighbor. The upper part shows the vector encoding of a NAS-Bench-201 architecture (left) and its radius-1 neighbor (right). The lower part shows the graph of the NAS-Bench-201 architecture (left) and one of its radius-1 neighbors (right). The neighbor architecture is obtained by adding a new connection with a random possible operation from node 1 to node 2. This corresponds to updating the 3rd element in the vector encoding.

4.1.1 Architecture neighborhood definition

Cell-based neural architectures can be represented as sequences of length L of natural numbers, where each number corresponds to a specific operation. We define the set of possible operations as $\mathcal{O} = \{1, \dots, k\}$, where k is the total number of admissible operations. An architecture can be expressed as a sequence (c_1, c_2, \dots, c_L) , where each c_i is an element of the set \mathcal{O} . To define architecture neighborhoods within NAS-Bench-201 and DARTS search spaces, we formalize an approach based on minimal modifications to these sequences. We define the radius \mathcal{R} in architecture space as the number of minimal modifications applied to distinct elements of an architecture, and a radius- \mathcal{R} neighbor as an architecture obtained by performing \mathcal{R} such modifications starting from an initial configuration.

In NAS-Bench-201, each NN architecture is represented by one type of cell, i.e. only one sequence. For example, a radius-1 neighbor is obtained by modifying a single integer in the sequence, effectively altering one operation in the cell, as illustrated in Fig. 1. In contrast, in DARTS cells are represented using adjacency matrices. The element at position (i, j) in the matrix corresponds to the operation connecting node i to node j , with a zero value indicating that there is no connection. To generate a radius-1 neighbor, we apply a minimal modification to the adjacency matrix, which can be one

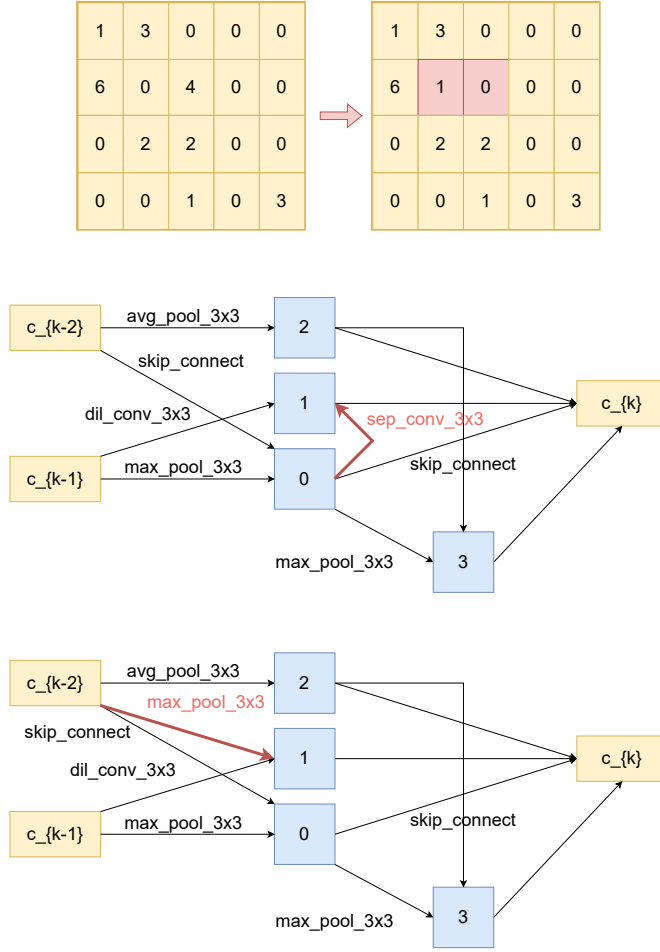


Figure 2: Example of a DARTS architecture and one of its radius-1 neighbor. The upper part shows the adjacency matrices of the DARTS architecture (left) and its radius-1 neighbor (right). The two lower graphs represent the DARTS architecture (up) and its radius-1 neighbor (down) corresponding to their adjacency matrices. The neighbor architecture is obtained by removing the connection from intermediate node 0 to node 1 and adding a new connection from the input node c_{k-2} to intermediate node 1. This corresponds to updating the elements in positions (1, 1) and (1, 2) in the matrix.

of the following two possible actions: (i) Operation Change: Replacing an operation in an existing edge; (ii) Connection Adjustment: Removing an edge to a node and adding a new connection with a randomly selected operation, ensuring each node maintains exactly two predecessors. A radius-1 neighbor is thus obtained by making a single, minimal change, either by modifying an operation or by adjusting connectivity. An illustration of the process (ii), Connection Adjustment, is provided in Fig. 2.

The equivalent integer sequence representation of the resulting perturbed adjacency matrix can be recovered by extracting the meaningful elements where $j - i \leq 1$ for $i = 0, \dots, M - 1$, where M is the number of intermediate nodes. Since DARTS architectures consist of both a normal cell and a reduction cell (each represented by a distinct adjacency matrix), modifications are applied randomly to one of the two matrices. Using this architecture neighborhood definition, we can construct a *neighbor tree*, where level \mathcal{R} consists of all architectures obtained through \mathcal{R} distinct modifications from an initial architecture (i.e., all architectures at radius \mathcal{R} from the root). Modifications that reverse previous changes are not allowed. An example of a neighbor tree is shown in the upper part of Fig. 3.

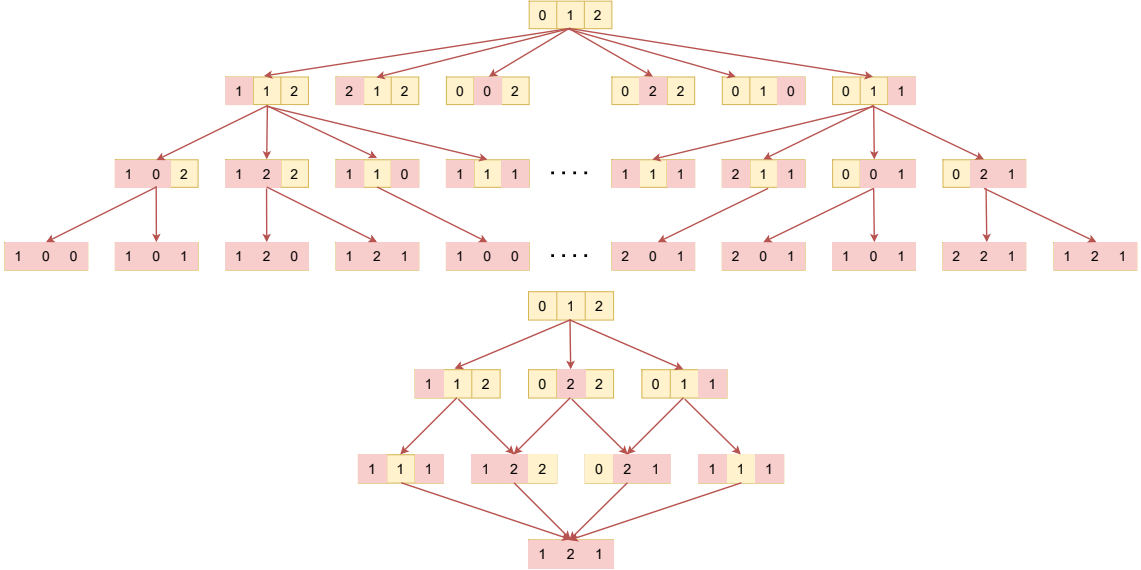


Figure 3: (Up) Visualization of a *neighbor tree* illustrating the neighborhood relationships for sequences of length 3 over a set of operations of length 3 and whose root is the initial configuration $[0, 1, 2]$. (Down) Visualization of a *path tree* with a sequence of length 3 and a set of operations of length 3 from $[0, 1, 2]$ to $[1, 2, 1]$ - i.e. two architectures at maximal radius.

4.1.2 Paths in Neural Architecture Space

We introduce a methodology for constructing paths between NN architectures. Given two sequences representing the configurations of two architectures, the path between them is identified through a search tree - illustrated at the left of Fig. 3 - that systematically connects the two networks through all the shortest possible paths between them. In this path-identifying search tree, each level consists of architectures obtained by incrementally modifying the configurations at the higher level in order to approach the target configuration. For instance, in NAS-Bench-201, an action consists of updating a single element in the current configuration to match the corresponding element in the target configuration. This process can be seen as a constrained variant of the neighbor tree, introduced in Section 4.1.1, where the set of possible moves is restricted to those that directly transition toward the target architecture. Once the path tree is constructed, we derive the accuracy path by considering the accuracies of the two endpoint architectures and computing the average accuracy of unique architectures (i.e., duplicate occurrences are counted only once) at each level of the tree (i.e., we average accuracy over all the distinct architectures over all possible shortest paths connecting the two endpoint networks). This approach provides a structured way to analyze accuracy transitions along paths in the neural architecture space.

4.2 The A²M Algorithm

We introduce A²M, a novel and *general* algorithmic framework introducing a novel formulation of the DARTS gradient update step in the *architecture* space, specifically tailored to bias the search process towards flat architecture neighborhoods. As we show in this paper, our architecture gradient step formulation *can be easily applied to most DARTS-based methods*. Our update step is analytically derived introducing the Sharpness-Aware Minimization (SAM) [26] update step, originally formulated in weight space (and in its unnormalized variant USAM [32], Eq. (7)), in the DARTS bi-level optimization problem, Eqs. 2. See Appendix A for the full gradient update derivation. In our approach, flatness is optimized exclusively on the architecture parameters α , resulting in the A²M update formula:

$$\nabla_{\alpha} \mathcal{L}_{\text{val}}(w^*(\alpha), \alpha) \approx \nabla_{\tilde{\alpha}_{\xi=0}} \mathcal{L}_{\text{val}}(w, \tilde{\alpha}_{\xi=0}) + \rho_{\alpha} \frac{\nabla_{\alpha_{\xi=0}^+} \mathcal{L}_{\text{val}}(w, \alpha_{\xi=0}^+) - \nabla_{\alpha_{\xi=0}^-} \mathcal{L}_{\text{val}}(w, \alpha_{\xi=0}^-)}{2\epsilon} \quad (8)$$

with $\alpha_{\xi=0}^{\pm} = \alpha \pm \epsilon \nabla_{\tilde{\alpha}_{\xi=0}} \mathcal{L}_{\text{val}}(w, \tilde{\alpha}_{\xi=0})$; $\tilde{\alpha}_{\xi=0} = \alpha + \rho_{\alpha} \nabla_{\alpha} \mathcal{L}_{\text{val}}(w, \alpha)$.

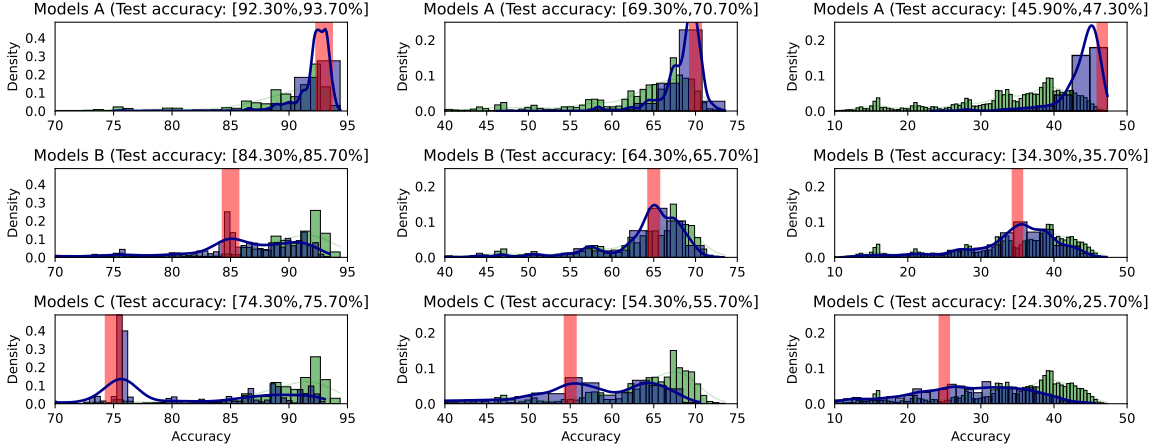


Figure 4: Histogram of test accuracies over radius-1 neighborhoods on NAS-Bench-201 and on CIFAR-10 (left), CIFAR-100 (middle) and ImageNet16-120 (right), for different accuracy ranges of reference architectures in the search space. The red shaded area refers to the range of test accuracies of the reference architectures (also reported in each subplot title). For each dataset, three accuracy ranges for the reference architecture were identified (corresponding to high, medium, and low performance), according to the difficulty of the dataset. The green distribution refers to the accuracies over the whole search space, while the blue one refers to the accuracies over the radius-1 neighborhoods only. The blue histograms reveal that radius-1 neighborhoods tend to have similar accuracies to their reference architectures, independently from the evident bias of the search space towards well-performing architectures revealed by the green histograms. Architectures with similar accuracies tend to geometrically cluster together, and there exist flat basins of architectures in the accuracy landscape.

This redefinition of the DARTS architecture gradient update step can be easily integrated as a plug-in into other DARTS-based algorithms, non-trivially modifying the architecture parameters update rule rather than randomly perturbing them. Unlike most prior works, which focus on enhancing DARTS through the introduction of additional regularization terms, and as can be seen from Eq. (8), our approach operates at a principled, flatness-enhancing level by introducing only one additional hyperparameter ρ_α related to the radius of the architecture neighborhood over which the optimization is performed.

5 Experimental Results

In this section, we present our experimental investigation, aiming to elucidate the geometrical properties of the NAS-Bench-201 and DARTS search spaces and to evaluate the effectiveness of A^2M in enhancing DARTS-based methods. We evaluate our methods on three benchmark datasets: CIFAR-10 [34], CIFAR-100 [34], and ImageNet16-120. CIFAR-10 and CIFAR-100 [34] consist of 32×32 color images, representing 10 and 100 classes, respectively. Each dataset contains 60,000 images, split into 50,000 training images and 10,000 test images. ImageNet16-120 [35] is a downsized version of the ImageNet dataset specifically designed for NAS evaluation, consisting of 16×16 color images spanning 120 object classes. It contains 151,700 training images and 6,000 test images.

5.1 Investigation of Local Properties and Flatness in Architecture Space

To shed light on the structural properties of the NAS-Bench-201 search space, we analyze the distribution of accuracies of architectures that are radius-1 neighbors of a set of reference architectures within a selected accuracy range. Specifically, we consider architectures that differ by a single operation and visualize their accuracy distributions, as shown in Fig. 4). For each data set (CIFAR-10, CIFAR-100, and ImageNet-16-120), we select three reference architectures representing high, medium, and low-performance models (top to bottom panel rows in Fig. 4). The shaded red area in each histogram highlights the accuracy range of the reference architectures, while the overall accuracy distribution across all NAS-Bench-201 architectures is shown in green.

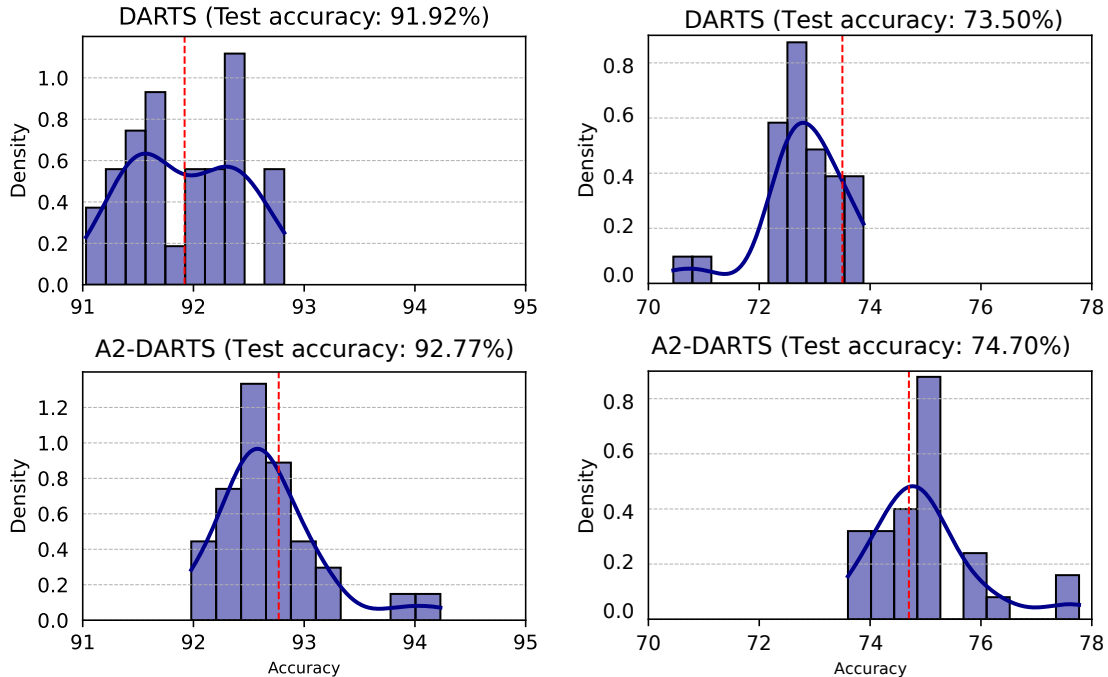


Figure 5: Histogram of test accuracies of radius-1 neighbors of a neural network architecture found by DARTS (upper panels) and A²-DARTS (lower panels) on CIFAR-10 (left column) and CIFAR-100 (right column). To obtain each histogram, 30 architectures have been sampled perturbing at random at radius 1 the initial configuration (whose accuracy is shown by the dashed red line), and trained until a fix loss threshold. We observe a local property around all initial architectures, with their neighbors taking accuracy values close to them. The highest accuracy networks cluster together, highlighting the presence of a flat region in neural architecture space.

Our results indicate strong locality properties in the architecture space: neighboring architectures tend to exhibit similar accuracy levels, that cannot be attributed to the evident bias of the search space towards high-performing architectures. Across all datasets, architectures have a consistent sequence length (i.e., the number of edges) of $L = 6$ and a set of $k = 5$ possible operations. These findings show that architectures with similar performances form clusters within the NAS-Bench-201 search space, resulting in a flat loss landscape in high-performance regions. This flatness property implies that small architecture modifications to well-performing architectures do not significantly degrade performance. Additional results for radius-2 and radius-3 neighborhoods are provided in Appendix C.1.

We extend this locality analysis to the more complex DARTS search space, where $L = 14$ and $k = 8$, and observe similar patterns (see Fig. 5 for the corresponding accuracy histograms on CIFAR-10 and CIFAR-100). For this experiment, we cannot rely on a tabular dataset as in the Nas-Bench-201 case, therefore we select two neural architectures obtained by DARTS and A²M respectively as reference models, and sample 30 random radius-1 neighbors using the procedure described in Sec. 4.1.1. For computational reasons, we terminate training early (typically between 50-70 epochs) once a predefined training loss is reached (0.43 for CIFAR-10 and 1.0 for CIFAR-100), in line with well-established procedures in flatness literature [36]. This loss value ensures that the models achieve sufficiently accurate performance while reducing the significant computational overhead necessary to optimize the entire architecture neighborhood. While this approach is viable on CIFAR-10 and CIFAR-100, it is not on ImageNet-16-120 where each architecture requires full training in order to reach a stable accuracy value. The results for DARTS on CIFAR-10 and CIFAR-100, shown in Fig. 5, confirm the presence of locality and flatness in the DARTS architecture space. This reinforces the potential for gradient-based NAS methods to efficiently navigate the architecture space targeting flat regions. Additional results for radius-2 and radius-3 neighborhoods on DARTS and on CIFAR-10 and CIFAR-100 are included in Appendix C.1.

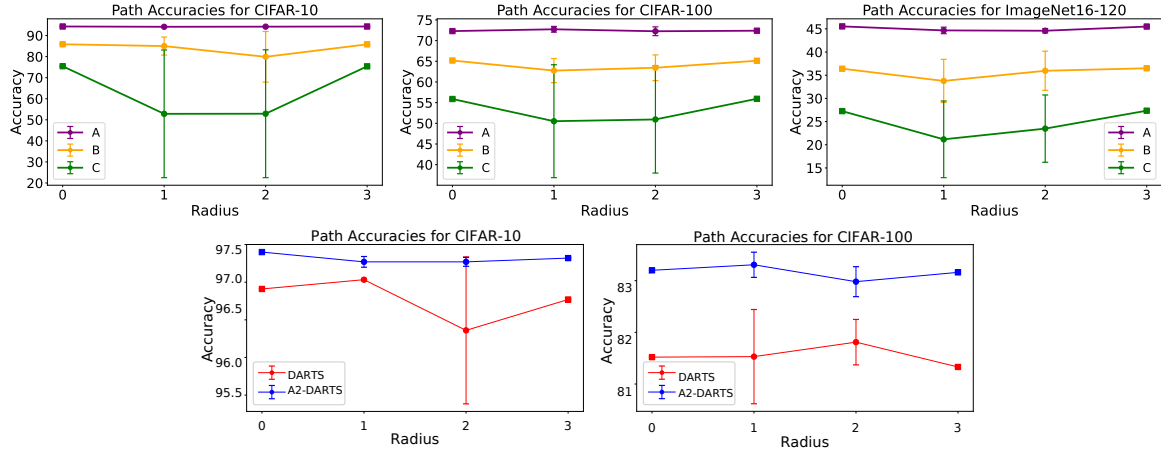


Figure 6: (Upper panels) Paths between architectures on NAS-Bench-201 on (a) CIFAR-10; (b) CIFAR-100; (c) ImageNet16-120. The barriers corresponding to the three paths (from top to bottom) are respectively equal to (a) 0.24, 22.52, 54.14; (b) 1.74, 4.93, 21.56; (c) 1.42, 7.11, 10.86. (Lower panels) Paths between architectures on DARTS on (a) CIFAR-10; and (b) CIFAR-100. We selected a model found by DARTS and A²-DARTS and a radius-3 neighbor with similar accuracy respectively to compute paths in this case. The barriers corresponding to paths between DARTS and A²-DARTS models are respectively (a) 1.99 and 0.15; (b) 1.23 and 0.63. While higher-performing architectures exhibit flatter paths between them, lower-performing ones are more isolated, showing higher accuracy barriers.

5.1.1 Neural Architecture Paths

For each dataset, we analyze the paths connecting architectures with three different test accuracy levels. This allows us to examine the presence of accuracy barriers between architectures with different performance levels. Each path connects an architecture \mathcal{A}_A to a radius-3 neighbor \mathcal{A}_B with similar test accuracy, following definitions in Sec. 4.1.1. In Fig. 6, we also report the normalized accuracy barrier, defined as: $\frac{1}{2}(\text{Acc}(\mathcal{A}_A) + \text{Acc}(\mathcal{A}_B)) - \min_{[\mathcal{A}_A, \mathcal{A}_B]} \text{Acc}(\mathcal{A}_C)$ where $\text{Acc}(\mathcal{A}_A)$ represents the test accuracy of architecture \mathcal{A}_A , and $[\mathcal{A}_A, \mathcal{A}_B]$ denotes the path connecting architectures \mathcal{A}_A and \mathcal{A}_B .

For NAS-Bench-201, we select three distinct accuracy levels for each dataset, corresponding to high, medium, and low-performing models relative to the dataset’s difficulty. Our objective is to verify whether higher-performing architectures exhibit lower barriers, indicating a smoother architecture landscape. In Fig. 6, we refer to these architectures as Model A, Model B, and Model C, listed in decreasing order of test accuracy. We construct a path (see Sec. 4.1.2) starting at each model, and ending at a selected architecture from the search space corresponding to a radius-3 neighbor with similar accuracy.

The identified accuracy levels for each dataset are:

- CIFAR-10 - Model A: 94.3%, Model B: 85.86%, Model C: 75.44%;
- CIFAR-100 - Model A: 72.30%, Model B: 65.19%, Model C: 55.88%;
- ImageNet16-120 - Model A: 45.53%, Model B: 36.41%, Model C: 27.26%.

As shown in the upper panels of Fig 6, the paths between low-performing architectures encounter higher accuracy barriers compared to those between high-performing architectures, which exhibit smoother paths, confirming the flatness properties of the search space, and the fact that lower-performing architectures are more isolated.

For the DARTS search space, we select two accuracy levels by considering architectures obtained from separate runs of DARTS and A²M applied to pure DARTS (A²-DARTS). These models were evaluated on CIFAR-10 and CIFAR-100. As discussed in Sec. 5, we did not analyze ImageNet-16-120 due to its computational demands. To compute the paths and the barriers, instead of selecting a predefined radius-3 neighbor, which was possible in NAS-Bench-201, we identify a neighbor with a similar test accuracy after partial training, truncated at a fixed train loss. This selected neighbor was

then fully trained to obtain its final accuracy. All models maintained comparable accuracy levels even after full training.

The identified accuracy levels are:

- CIFAR-10 - DARTS: 96.91%, A²-DARTS: 97.40%;
- CIFAR-100 - DARTS: 81.52%, A²-DARTS: 83.20%.

Results are shown in the lower panels of Fig 6. Our findings validate the flatness property of the architecture landscape in both NAS-Bench-201 and DARTS search spaces. Furthermore, the methodology we propose is not limited to cell-based search spaces but could be extended to broader NAS formulations, including supernet-based search spaces such as Once-For-All (OFA) [37].

5.2 A²M Algorithm Evaluation

To demonstrate the generalization improvements introduced by A²M, we evaluate its impact on seven state-of-the-art DARTS-based methods: DARTS (1st order) [6], β -DARTS [11], Λ -DARTS [30], DARTS-PT² [9], DARTS- [10], SDARTS-RS [38], and PC-DARTS [29]. We evaluate these methods and their A²-enhanced variants on both NAS-Bench-201 and DARTS search spaces across three benchmark datasets: CIFAR-10, CIFAR-100, and ImageNet-16-120. We highlight that the architecture search is conducted only on CIFAR-10, and the discovered genotype is subsequently evaluated on the other datasets. To determine the optimal ρ_α value for A²M, we perform a search on CIFAR-10 only, reported in Appendix C.2. A²M introduces only a modest increase in search cost, ranging between $\times 1.1$ and $\times 1.3$ times the one of the original methods. For each experiment, we computed the results for 5 different seeds and reported the average value and the standard deviation.

Table 1: Comparison of test accuracy on NAS-Bench-201 (upper table) and DARTS search space (lower table) across CIFAR-10, CIFAR-100, and ImageNet-16-120 datasets for multiple SotA methods, showing standard and A²-enhanced results. The results are averaged over 5 different seeds. *DARTS and A²-DARTS have been run without data augmentation on the validation set on NAS-Bench-201. The best result for each search space is reported in **bold**. *Optimal* refers to the best NN of NAS-Bench-201. *Avg Test Acc* refers to the average test accuracy by averaging over all the reported methods and search space for each dataset. *Avg Gain* refers to the gain in *Avg Test Acc* for each dataset.

Model	CIFAR-10 Test Acc (%)		CIFAR-100 Test Acc (%)		ImageNet16-120 Test Acc (%)	
	Standard	A ² -	Standard	A ² -	Standard	A ² -
DARTS (1st)* [6]	72.85±35.21	92.39±0.52	49.44±27.39	68.79±1.61	26.24±15.33	41.88±2.21
β -DARTS [11]	94.15±0.29	94.15±0.29	72.77±0.83	72.77±0.83	45.66±0.92	45.66±0.92
Λ -DARTS [30]	92.69±1.90	93.96±0.47	69.99±3.78	72.05±1.73	43.00±3.36	45.27±1.27
DARTS-PT[9]	88.40±0.0	92.31±0.0	61.35±0.0	68.19±0.0	34.62±0.0	41.24±0.0
DARTS- [10]	93.76±0.43	93.76±0.43	71.11±1.60	71.11±1.60	41.44±0.90	41.44±0.90
SDARTS-RS [8]	80.57±0.30	84.33±0.18	47.93±0.43	54.96±0.33	26.29±0.72	25.62±0.26
PC-DARTS [29]	70.92±0.35	91.95±0.16	38.97±0.80	66.47±0.40	18.41±0.70	39.59±0.97
OPTIMAL [21]		94.37		73.51		46.71
DARTS (1st) [6]	97.00±0.14	97.20±0.15	82.30±0.30	82.50±0.79	53.06±0.53	55.03±0.37
β -DARTS [11]	96.83±0.15	96.94±0.16	81.85±0.68	82.48±0.27	53.92±0.47	54.45±0.42
Λ -DARTS [30]	97.05±0.39	97.14±0.32	82.92±0.32	83.16±0.42	53.62±0.48	58.92±0.33
DARTS-PT [9]	97.36±0.09	97.42±0.07	83.53±0.23	83.60±0.21	54.00±0.39	54.28±0.35
DARTS- [10]	97.30±0.15	97.36±0.12	82.43±0.31	82.32±0.24	53.78±0.51	54.32±0.43
SDARTS-RS [38]	97.33±0.03	97.38±0.04	82.50±0.22	82.67±0.24	55.48±0.30	55.70±0.38
PC-DARTS [29]	97.15±0.18	97.20±0.13	82.18±0.27	82.60±0.25	57.38±0.46	54.33±0.54
AVG TEST ACC (%)	90.95	94.54	70.66	75.26	44.06	47.70
AVG GAIN (%)		+3.60		+4.60		+3.64

²For A²-DARTS-PT, we apply A²M both during the architecture search phase and the final model selection phase, where a tuning of the supernet is performed.

5.3 Results on NAS-Bench-201 Search Space

For experiments in the NAS-Bench-201 search space, we follow the original search settings of each DARTS-based method. However, for SDARTS-RS and PC-DARTS, we adopt the DARTS search settings from [21], as these methods were not originally evaluated on NAS-Bench-201. Additionally, for Λ -DARTS, we limit the search phase to 50 epochs to ensure consistency with the search runs of other NAS methods [30]. The results are presented in the first section of Table 1, where we compare test accuracies between the original methods (labeled as Standard) and their A^2 -enhanced variants for each dataset. As in prior DARTS-based studies, validation accuracies are reported separately in Appendix C.3. To provide an upper bound on achievable performance within the search space, we include the optimal architecture in NAS-Bench-201 as a baseline, labeled OPTIMAL. As shown in the upper part of Table 1, A^2 M enhances performance across all evaluated methods apart from β -DARTS and DARTS-, where performance remains unchanged. We observed that on NAS-Bench-201, DARTS and A^2 -DARTS consistently yield improved performance when data augmentation is disabled on the validation set, as discussed in Appendix C.4. We report the results of both algorithms with this setting. In particular, results show a huge improvement in DARTS and PC-DARTS, with a maximum of a more than double ($\times 2.15$) increase in accuracy of PC-DARTS on ImageNet-16-120.

5.4 Results on DARTS Search Space

For experiments conducted in the DARTS search space, we maintain the original search settings of each DARTS-based method to ensure consistency. The evaluation settings for all discovered networks align with the DARTS evaluation protocol for CIFAR-10 [6]. Moreover, the architecture search is performed on CIFAR-10, and the resulting genotype is then evaluated on various datasets by training the corresponding neural networks from scratch. The comparison results are summarized in the lower part of Table 1, which reports the test accuracies for both the original methods (labeled as Standard) and their A^2 -enhanced variants across all datasets. For β -DARTS, we reproduced the procedure based on its original GitHub repository to the best of our efforts, with detailed reproduction steps outlined in Appendix C.5.

The results in the lower part of Table 1 demonstrate that A^2 M improves performance across all evaluated methods on all datasets, with the exception of DARTS- on CIFAR-100 and PC-DARTS on ImageNet16-120. We highlight that the *best methods in terms of test accuracy of the final model are all A^2 -enhanced ones*: A^2 -DARTS-PT on CIFAR-10 and CIFAR-100 and A^2 - Λ -DARTS on ImageNet16-120.

6 Conclusions

By conducting an extensive and quantitative analysis of the geometric properties of architecture spaces used in differentiable NAS methods, such as NAS-Bench-201 and DARTS, we establish clear parallels between architecture landscapes and loss landscapes in weight space. Notably, by studying architecture neighborhoods and introducing a principled way of computing paths in the architecture landscape, we show that both search spaces exhibit locality and flatness properties, with flat regions corresponding to clusters of high-performing architectures, while architectures with lower performances are separated by higher accuracy barriers, and therefore more isolated. Our results shed light on the relationship between the geometrical properties of the architecture space and network performance, and yield practical implications for improving the effectiveness of differentiable NAS optimization algorithms.

A^2 M, our proposed algorithmic framework introducing a new architecture gradient update step in the DARTS bi-level optimization problem, can be easily applied to DARTS-based methods, and shows substantial performance gains obtained on several benchmark datasets, several DARTS-based methods and search spaces, demonstrating the practical benefits of explicitly targeting flat regions in the architecture space. In fact, by explicitly targeting flatness, A^2 M consistently outperforms state-of-the-art DARTS-based algorithms, leading to improved generalization and variance reduction.

These results contribute to a deeper understanding of NAS search spaces and provide valuable insights for developing more robust and efficient NAS strategies. Our proposed architecture landscape investigation techniques and flatness-targeting algorithms have the potential to be extended and to yield performance improvements even in other NAS optimization strategies, including supernet-based

search spaces, zero-shot methods, or specific application tasks such as NAS for Out-Of-Distribution robustness and adaptivity to concept drift.

Acknowledgements

This paper is supported by PNRR-PE-AI FAIR project funded by the NextGeneration EU program.

References

- [1] M. Poyser and T. P. Breckon, “Neural architecture search: A contemporary literature review for computer vision applications,” *Pattern Recognition*, vol. 147, p. 110052, 2024.
- [2] M. Gambella, A. Falcetta, and M. Roveri, “CNAS: Constrained neural architecture search,” in *2022 IEEE International Conference on Systems, Man, and Cybernetics (SMC)*, IEEE, 2022.
- [3] H. Benmeziiane, K. El Maghraoui, H. Ouarnoughi, S. Niar, M. Wistuba, and N. Wang, “Hardware-Aware Neural Architecture Search: Survey and Taxonomy,” in *Proceedings of the Thirtieth International Joint Conference on Artificial Intelligence*, (Montreal, Canada), pp. 4322–4329, International Joint Conferences on Artificial Intelligence Organization, Aug. 2021.
- [4] D. Ashlock, *Evolutionary Computation for Modeling and Optimization*. Springer Publishing Company, Incorporated, 1st ed., 2010.
- [5] R. Sutton and A. Barto, “Reinforcement learning: An introduction,” *IEEE Transactions on Neural Networks*, vol. 9, no. 5, pp. 1054–1054, 1998.
- [6] H. Liu, K. Simonyan, and Y. Yang, “DARTS: Differentiable architecture search,” in *International Conference on Learning Representations*, 2019.
- [7] A. Zela, T. Elsken, T. Saikia, Y. Marrakchi, T. Brox, and F. Hutter, “Understanding and robustifying differentiable architecture search,” in *International Conference on Learning Representations*, 2020.
- [8] X. Chen and C.-J. Hsieh, “Stabilizing differentiable architecture search via perturbation-based regularization,” in *Proceedings of the 37th International Conference on Machine Learning* (H. D. III and A. Singh, eds.), vol. 119 of *Proceedings of Machine Learning Research*, pp. 1554–1565, PMLR, 13–18 Jul 2020.
- [9] R. Wang, M. Cheng, X. Chen, X. Tang, and C.-J. Hsieh, “Rethinking architecture selection in differentiable NAS,” in *International Conference on Learning Representations*, 2021.
- [10] X. Chu, X. Wang, B. Zhang, S. Lu, X. Wei, and J. Yan, “{DARTS}-: Robustly stepping out of performance collapse without indicators,” in *International Conference on Learning Representations*, 2021.
- [11] P. Ye, B. Li, Y. Li, T. Chen, J. Fan, and W. Ouyang, “ β -darts: Beta-decay regularization for differentiable architecture search,” in *2022 IEEE/CVF Conference on Computer Vision and Pattern Recognition (CVPR)*, pp. 10864–10873, 2022.
- [12] P. Ye, T. He, B. Li, T. Chen, L. Bai, and W. Ouyang, “ β -darts++: Bi-level regularization for proxy-robust differentiable architecture search,” 2023.
- [13] X. Zhu, J. Li, Y. Liu, and W. Wang, “Improving differentiable architecture search via self-distillation,” *Neural Networks*, vol. 167, pp. 656–667, 2023.
- [14] H. Li, Z. Xu, G. Taylor, C. Studer, and T. Goldstein, “Visualizing the loss landscape of neural nets,” in *Advances in neural information processing systems*, pp. 6389–6399, 2018.
- [15] M. Gambella, F. Pittorino, and M. Roveri, “Flatnas: optimizing flatness in neural architecture search for out-of-distribution robustness,” in *2024 International Joint Conference on Neural Networks (IJCNN)*, pp. 1–8, 2024.

- [16] B. L. Annesi, C. Lauditi, C. Lucibello, E. M. Malatesta, G. Perugini, F. Pittorino, and L. Saglietti, “Star-shaped space of solutions of the spherical negative perceptron,” *Phys. Rev. Lett.*, vol. 131, p. 227301, Nov 2023.
- [17] C. Lucibello, F. Pittorino, G. Perugini, and R. Zecchina, “Deep learning via message passing algorithms based on belief propagation,” *Machine Learning: Science and Technology*, vol. 3, p. 035005, jul 2022.
- [18] C. Baldassi, F. Pittorino, and R. Zecchina, “Shaping the learning landscape in neural networks around wide flat minima,” *Proceedings of the National Academy of Sciences*, vol. 117, no. 1, pp. 161–170, 2020.
- [19] X. Wang, S. Cao, M. Li, and K. M. Kitani, “Neighborhood-Aware Neural Architecture Search,” Oct. 2021. arXiv:2105.06369 [cs].
- [20] C. White, S. Nolen, and Y. Savani, “Exploring the loss landscape in neural architecture search,” in *Conference on Uncertainty in Artificial Intelligence*, 2020.
- [21] X. Dong and Y. Yang, “Nas-bench-201: Extending the scope of reproducible neural architecture search,” in *International Conference on Learning Representations (ICLR)*, 2020.
- [22] F. Pittorino, C. Lucibello, C. Feinauer, G. Perugini, C. Baldassi, E. Demyanenko, and R. Zecchina, “Entropic gradient descent algorithms and wide flat minima,” in *International Conference on Learning Representations*, 2021.
- [23] F. Pittorino, C. Lucibello, C. Feinauer, G. Perugini, C. Baldassi, E. Demyanenko, and R. Zecchina, “Entropic gradient descent algorithms and wide flat minima*,” *Journal of Statistical Mechanics: Theory and Experiment*, vol. 2021, p. 124015, dec 2021.
- [24] F. Pittorino, A. Ferraro, G. Perugini, C. Feinauer, C. Baldassi, and R. Zecchina, “Deep networks on toroids: Removing symmetries reveals the structure of flat regions in the landscape geometry,” in *Proceedings of the 39th International Conference on Machine Learning* (K. Chaudhuri, S. Jegelka, L. Song, C. Szepesvari, G. Niu, and S. Sabato, eds.), vol. 162 of *Proceedings of Machine Learning Research*, pp. 17759–17781, PMLR, 17–23 Jul 2022.
- [25] F. Pittorino, A. Ferraro, G. Perugini, C. Feinauer, C. Baldassi, and R. Zecchina, “Deep networks on toroids: removing symmetries reveals the structure of flat regions in the landscape geometry*,” *Journal of Statistical Mechanics: Theory and Experiment*, vol. 2022, p. 114007, nov 2022.
- [26] P. Foret, A. Kleiner, H. Mobahi, and B. Neyshabur, “Sharpness-aware minimization for efficiently improving generalization,” in *International Conference on Learning Representations*, 2021.
- [27] X. Chu, T. Zhou, B. Zhang, and J. Li, “Fair darts: Eliminating unfair advantages in differentiable architecture search,” in *European conference on computer vision*, pp. 465–480, Springer, 2020.
- [28] H. Liang, S. Zhang, J. Sun, X. He, W. Huang, K. Zhuang, and Z. Li, “Darts+: Improved differentiable architecture search with early stopping,” *arXiv preprint arXiv:1909.06035*, 2019.
- [29] Y. Xu, L. Xie, X. Zhang, X. Chen, G.-J. Qi, Q. Tian, and H. Xiong, “Pc-darts: Partial channel connections for memory-efficient architecture search,” in *International Conference on Learning Representations (ICLR)*, 2020.
- [30] S. Movahedi, M. Adabinejad, A. Imani, A. Keshavarz, M. Dehghani, A. Shakery, and B. N. Araabi, “ λ -DARTS: Mitigating performance collapse by harmonizing operation selection among cells,” in *The Eleventh International Conference on Learning Representations*, 2023.
- [31] Y. Shu, W. Wang, and S. Cai, “Understanding architectures learnt by cell-based neural architecture search,” in *International Conference on Learning Representations*, 2020.
- [32] M. Andriushchenko and N. Flammarion, “Towards understanding sharpness-aware minimization,” in *Proceedings of the 39th International Conference on Machine Learning*, 2022.
- [33] J. Lorraine, P. Vicol, and D. Duvenaud, “Optimizing millions of hyperparameters by implicit differentiation,” in *AISTATS*, pp. 1540–1552, 2020.

- [34] A. Krizhevsky, “Learning multiple layers of features from tiny images,” 2009.
- [35] P. Chrabaszcz, I. Loshchilov, and F. Hutter, “A downsampled variant of imagenet as an alternative to the cifar datasets,” *ArXiv*, vol. abs/1707.08819, 2017.
- [36] Y. Jiang*, B. Neyshabur*, H. Mobahi, D. Krishnan, and S. Bengio, “Fantastic generalization measures and where to find them,” in *International Conference on Learning Representations*, 2020.
- [37] H. Cai, C. Gan, T. Wang, Z. Zhang, and S. Han, “Once-for-All: Train One Network and Specialize it for Efficient Deployment,” Apr. 2020. arXiv:1908.09791 [cs, stat].
- [38] X. Chen and C.-J. Hsieh, “Stabilizing differentiable architecture search via perturbation-based regularization,” in *Proceedings of the 37th International Conference on Machine Learning (ICML)*, pp. 1554–1565, 2020.

A Warm up: DARTS bi-level optimization and USAM update

In this section, we provide additional background on the DARTS bi-level optimization problem and on the USAM update, that will both be instrumental to analytically derive our newly proposed A²M architecture gradient update, introduced in Eq. (8).

A.1 DARTS Approximated Gradient

By defining the one-weight-step approximated gradient:

$$w'(\alpha) = w - \xi \nabla_w \mathcal{L}_{train}(w, \alpha) \quad (9)$$

and the chain rule

$$\nabla_\alpha \mathcal{L}(w'(\alpha)) = \nabla_\alpha w'(\alpha) \nabla_{w'} \mathcal{L}(w') \quad (10)$$

we can write the one-weight-step approximated DARTS gradient as:

$$\nabla_\alpha \mathcal{L}_{val}(w^*(\alpha), \alpha) \approx \nabla_\alpha \mathcal{L}_{val}(w'(\alpha), \alpha) \quad (11)$$

$$= \nabla_\alpha \mathcal{L}_{val}(w', \alpha) + \nabla_\alpha w'(\alpha) \nabla_{w'} \mathcal{L}_{val}(w', \alpha) \quad (12)$$

$$= \nabla_\alpha \mathcal{L}_{val}(w', \alpha) + \nabla_\alpha (w - \xi \nabla_w \mathcal{L}_{train}(w, \alpha)) \nabla_{w'} \mathcal{L}_{val}(w', \alpha) \quad (13)$$

$$= \nabla_\alpha \mathcal{L}_{val}(w', \alpha) - \xi \nabla_{\alpha, w}^2 \mathcal{L}_{train}(w, \alpha) \nabla_{w'} \mathcal{L}_{val}(w', \alpha) \quad (14)$$

$$\approx \nabla_\alpha \mathcal{L}_{val}(w', \alpha) - \xi \left(\frac{\nabla_\alpha \mathcal{L}_{train}(w^+, \alpha) - \nabla_\alpha \mathcal{L}_{train}(w^-, \alpha)}{2\epsilon} \right) \quad (15)$$

where in Eq. (12) we have summed up the contributions to the gradient coming from the first and second argument of \mathcal{L}_{val} . for the derivative with respect to the second argument we have used the chain rule Eq.(10), and in Eq.(15) we have used the finite difference approximation

$$\nabla_{\alpha, w}^2 \mathcal{L}_{train}(w, \alpha) \approx \frac{\nabla_\alpha \mathcal{L}_{train}(w^+, \alpha) - \nabla_\alpha \mathcal{L}_{train}(w^-, \alpha)}{2\epsilon \nabla_{w'} \mathcal{L}_{val}(w', \alpha)} \quad (16)$$

with

$$w^\pm = w \pm \epsilon \nabla_{w'} \mathcal{L}_{val}(w', \alpha). \quad (17)$$

A.2 The USAM Update

We recall the USAM [32] gradient update. In USAM, the SAM gradient step is simplified by avoiding normalization, reducing computational complexity, and has been empirically shown to perform well [32]. Eq. (7) can be rewritten as:

$$\nabla f(x_k) \xrightarrow{USAM} \nabla f(x_k + \rho \nabla f(x_k)) \quad (18)$$

or

$$\nabla f(x_k) \xrightarrow{USAM} \nabla f(\tilde{x}_k(x_k)) \quad \text{with} \quad \tilde{x}_k(x_k) = x_k + \rho \nabla f(x_k) \quad (19)$$

B Derivation of the A²M Gradient Update

In this section, we derive our newly proposed A²M gradient update step, introduced in Eq. (8). As a preliminary step, let us write the USAM update specifically for α :

$$\nabla_\alpha \mathcal{L}_{val}(w'(\alpha), \alpha) \xrightarrow{USAM} \nabla_\alpha \mathcal{L}_{val}(w'(\tilde{\alpha}(\alpha)), \tilde{\alpha}(\alpha)) \quad (20)$$

where

$$\tilde{\alpha}(\alpha) = \alpha + \rho_\alpha \nabla_\alpha \mathcal{L}_{val}(w'(\alpha), \alpha) \quad (21)$$

$$= \alpha + \rho_\alpha \nabla_\alpha \mathcal{L}_{val}(w', \alpha) - \rho_\alpha \xi \left(\frac{\nabla_\alpha \mathcal{L}_{train}(w^+, \alpha) - \nabla_\alpha \mathcal{L}_{train}(w^-, \alpha)}{2\epsilon} \right) \quad (22)$$

where in Eq. (22) we have used Eq. (15).

B.1 Gradient With Respect To the First Argument

In order to obtain the total gradient, we have to differentiate $\mathcal{L}_{val}(\cdot, \cdot)$ separately with respect to its first and second argument and sum the two gradients. Let us calculate in this section the gradient with respect to the first argument, which involves the definition of $w'(\alpha)$ Eq. (9):

$$\nabla_{\alpha} \mathcal{L}_{val}(w'(\tilde{\alpha}(\alpha)), \tilde{\alpha}(\alpha)) \Big|_{1^{\text{st}} \text{ argument}} = (\nabla_{\alpha} w'(\tilde{\alpha}(\alpha))) \nabla_{w'} \mathcal{L}_{val}(w', \tilde{\alpha}) \quad (23)$$

$$= (\nabla_{\alpha} \tilde{\alpha}(\alpha)) \nabla_{\tilde{\alpha}} w'(\tilde{\alpha}) \nabla_{w'} \mathcal{L}_{val}(w', \tilde{\alpha}) \quad (24)$$

where

$$\nabla_{\alpha} \tilde{\alpha}(\alpha) = \nabla_{\alpha} \left(\alpha + \rho_{\alpha} \nabla_{\alpha} \mathcal{L}_{val}(w', \alpha) - \rho_{\alpha} \xi \left(\frac{\nabla_{\alpha} \mathcal{L}_{train}(w^+, \alpha) - \nabla_{\alpha} \mathcal{L}_{train}(w^-, \alpha)}{2\epsilon} \right) \right) \quad (25)$$

$$= 1 + \rho_{\alpha} \nabla_{\alpha}^2 \mathcal{L}_{val}(w', \alpha) - \rho_{\alpha} \xi \left(\frac{\nabla_{\alpha}^2 \mathcal{L}_{train}(w^+, \alpha) - \nabla_{\alpha}^2 \mathcal{L}_{train}(w^-, \alpha)}{2\epsilon} \right) \quad (26)$$

$$(27)$$

and

$$\nabla_{\tilde{\alpha}} w'(\tilde{\alpha}) = \nabla_{\tilde{\alpha}} (w - \xi \nabla_w \mathcal{L}_{train}(w, \tilde{\alpha})) \quad (28)$$

$$= \xi \nabla_{w, \tilde{\alpha}}^2 \mathcal{L}_{train}(w, \tilde{\alpha}) \quad (29)$$

so that we obtain

$$\begin{aligned} \nabla_{\alpha} \mathcal{L}_{val}(w'(\tilde{\alpha}(\alpha)), \tilde{\alpha}(\alpha)) \Big|_{1^{\text{st}} \text{ argument}} &= \left(1 + \rho_{\alpha} \nabla_{\alpha}^2 \mathcal{L}_{val}(w', \alpha) \right. \\ &\quad \left. - \rho_{\alpha} \xi \left(\frac{\nabla_{\alpha}^2 \mathcal{L}_{train}(w^+, \alpha) - \nabla_{\alpha}^2 \mathcal{L}_{train}(w^-, \alpha)}{2\epsilon} \right) \right) \xi \nabla_{w, \tilde{\alpha}}^2 \mathcal{L}_{train}(w, \tilde{\alpha}) \nabla_{w'} \mathcal{L}_{val}(w', \tilde{\alpha}). \end{aligned} \quad (30)$$

Therefore, as we uncover that this gradient is linear in the weight learning rate ξ , in the approximation in which it is set to $\xi = 0$, i.e. a DARTS-like first order approximation, the entire gradient of \mathcal{L}_{val} with respect to the first argument is set to zero and does not contribute to the A²M gradient.

B.2 Gradient With Respect To the Second Argument

Let us compute the gradient with respect to the second argument. We apply the chain rule to the second argument of $\mathcal{L}_{val}(\cdot, \cdot)$:

$$\nabla_{\alpha} \mathcal{L}_{val}(w'(\tilde{\alpha}(\alpha)), \tilde{\alpha}(\alpha)) \Big|_{2^{\text{nd}} \text{ argument}} = (\nabla_{\alpha} \tilde{\alpha}(\alpha)) \nabla_{\tilde{\alpha}} \mathcal{L}_{val}(w'(\tilde{\alpha}), \tilde{\alpha}) \quad (31)$$

such that

$$\nabla_{\alpha} \mathcal{L}_{val}(w'(\tilde{\alpha}(\alpha)), \tilde{\alpha}(\alpha)) = \quad (32)$$

$$= (\nabla_{\alpha} \tilde{\alpha}(\alpha)) \nabla_{\tilde{\alpha}} \mathcal{L}_{val}(w'(\tilde{\alpha}), \tilde{\alpha})$$

$$= \left(1 + \rho_{\alpha} \nabla_{\alpha}^2 \mathcal{L}_{val}(w', \alpha) - \rho_{\alpha} \xi \left(\frac{\nabla_{\alpha}^2 \mathcal{L}_{train}(w^+, \alpha) - \nabla_{\alpha}^2 \mathcal{L}_{train}(w^-, \alpha)}{2\epsilon} \right) \right) \nabla_{\tilde{\alpha}} \mathcal{L}_{val}(w'(\tilde{\alpha}), \tilde{\alpha})$$

$$= \nabla_{\tilde{\alpha}} \mathcal{L}_{val}(w'(\tilde{\alpha}), \tilde{\alpha}) \quad (33)$$

$$+ \left(\rho_{\alpha} \nabla_{\alpha}^2 \mathcal{L}_{val}(w', \alpha) - \rho_{\alpha} \xi \left(\frac{\nabla_{\alpha}^2 \mathcal{L}_{train}(w^+, \alpha) - \nabla_{\alpha}^2 \mathcal{L}_{train}(w^-, \alpha)}{2\epsilon} \right) \right) \nabla_{\tilde{\alpha}} \mathcal{L}_{val}(w'(\tilde{\alpha}), \tilde{\alpha})$$

Now we can apply the finite difference approximation to the terms

$$\nabla_{\alpha}^2 \mathcal{L}_{val}(w', \alpha) \approx \frac{\nabla_{\alpha} \mathcal{L}_{val}(w', \alpha_1^+) - \nabla_{\alpha} \mathcal{L}_{val}(w', \alpha_1^-)}{2\epsilon_1 \nabla_{\tilde{\alpha}} \mathcal{L}_{val}(w'(\tilde{\alpha}), \tilde{\alpha})} \quad (34)$$

$$\nabla_{\alpha}^2 \mathcal{L}_{train}(w^+, \alpha) \approx \frac{\nabla_{\alpha} \mathcal{L}_{train}(w^+, \alpha_2^+) - \nabla_{\alpha} \mathcal{L}_{train}(w^+, \alpha_2^-)}{2\epsilon_2 \nabla_{\tilde{\alpha}} \mathcal{L}_{val}(w'(\tilde{\alpha}), \tilde{\alpha})} \quad (35)$$

$$\nabla_{\alpha}^2 \mathcal{L}_{train}(w^-, \alpha) \approx \frac{\nabla_{\alpha} \mathcal{L}_{train}(w^-, \alpha_3^+) - \nabla_{\alpha} \mathcal{L}_{train}(w^-, \alpha_3^-)}{2\epsilon_3 \nabla_{\tilde{\alpha}} \mathcal{L}_{val}(w'(\tilde{\alpha}), \tilde{\alpha})} \quad (36)$$

where

$$\alpha_i^\pm = \alpha \pm \epsilon_i \nabla_{\tilde{\alpha}} \mathcal{L}_{val}(w'(\tilde{\alpha}), \tilde{\alpha}) \quad \text{for } i = 1, 2, 3 \quad (37)$$

such that finally we obtain that the gradient Eq. (32) is:

$$\nabla_{\alpha} \mathcal{L}_{val}(w'(\tilde{\alpha}(\alpha)), \tilde{\alpha}(\alpha)) = \quad (38)$$

$$\nabla_{\tilde{\alpha}} \mathcal{L}_{val}(w'(\tilde{\alpha}), \tilde{\alpha}) + \rho_{\alpha} \frac{\nabla_{\alpha} \mathcal{L}_{val}(w', \alpha^+) - \nabla_{\alpha} \mathcal{L}_{val}(w', \alpha^-)}{2\epsilon} + \quad (39)$$

$$- \rho_{\alpha} \xi \left(\frac{1}{2\epsilon} \left(\frac{\nabla_{\alpha} \mathcal{L}_{train}(w^+, \alpha^+) - \nabla_{\alpha} \mathcal{L}_{train}(w^+, \alpha^-)}{2\epsilon} - \frac{\nabla_{\alpha} \mathcal{L}_{train}(w^-, \alpha^+) - \nabla_{\alpha} \mathcal{L}_{train}(w^-, \alpha^-)}{2\epsilon} \right) \right). \quad (40)$$

We can obtain the DARTS-like first-order approximation by setting the weight learning rate ξ to zero and we obtain:

$$\nabla_{\alpha} \mathcal{L}_{val}(w'(\tilde{\alpha}(\alpha)), \tilde{\alpha}(\alpha)) = \nabla_{\alpha} \mathcal{L}_{val}(w, \tilde{\alpha}_{\xi=0}(\alpha)) \quad (41)$$

$$= \nabla_{\tilde{\alpha}_{\xi=0}} \mathcal{L}_{val}(w, \tilde{\alpha}_{\xi=0}) + \rho_{\alpha} \frac{\nabla_{\alpha} \mathcal{L}_{val}(w, \alpha_{\xi=0}^+) - \nabla_{\alpha} \mathcal{L}_{val}(w, \alpha_{\xi=0}^-)}{2\epsilon} \quad (42)$$

$$= \nabla_{\tilde{\alpha}_{\xi=0}} \mathcal{L}_{val}(w, \tilde{\alpha}_{\xi=0}) + \rho_{\alpha} \frac{\nabla_{\alpha_{\xi=0}^+} \mathcal{L}_{val}(w, \alpha_{\xi=0}^+) - \nabla_{\alpha_{\xi=0}^-} \mathcal{L}_{val}(w, \alpha_{\xi=0}^-)}{2\epsilon} (1 + \mathcal{O}(\epsilon)) \quad (43)$$

with

$$\alpha_{\xi=0}^\pm = \alpha \pm \epsilon \nabla_{\tilde{\alpha}_{\xi=0}} \mathcal{L}_{val}(w, \tilde{\alpha}_{\xi=0}) \quad (44)$$

$$\tilde{\alpha}_{\xi=0} = \alpha + \rho_{\alpha} \nabla_{\alpha} \mathcal{L}_{val}(w, \alpha) \quad (45)$$

which is the A²M formula reported in the main text, Eqs. (8).

By applying the perturbation only to α , we specifically target flatness in the architecture parameter space without increasing the computational burden significantly because the number of architecture parameters is significantly smaller than the number of network weights. The choice of ρ_{α} is critical; it controls the extent of the neighborhood considered for sharpness minimization. We select ρ_{α} based on validation performance, as shown in Appendix C.2. A²M is compatible with existing DARTS implementations and can be integrated with other NAS methods based on a continuous relaxation of the architecture space.

C Additional results

In this section, we report additional results and ablation studies.

C.1 Neighborhoods at the Extended Radii 2 and 3

We report test accuracy histograms computed respectively over neighborhoods at radius 2 and 3 in Figs. 7 and 8 for NAS-Bench-201 and in Figs. 9 and 10 for DARTS. Interestingly, we observe that in the Nas-Bench-201 case the accuracy distribution over the extended neighborhoods at radius 2 and 3 (blue) becomes similar to the distribution of the whole search space (green), due to the small size of the search space, and therefore it becomes impossible to observe architecture clustering. In contrast, in the DARTS search space which has a much bigger size, clustering and locality properties can be observed up to more extended neighborhoods of radius 2 and 3.

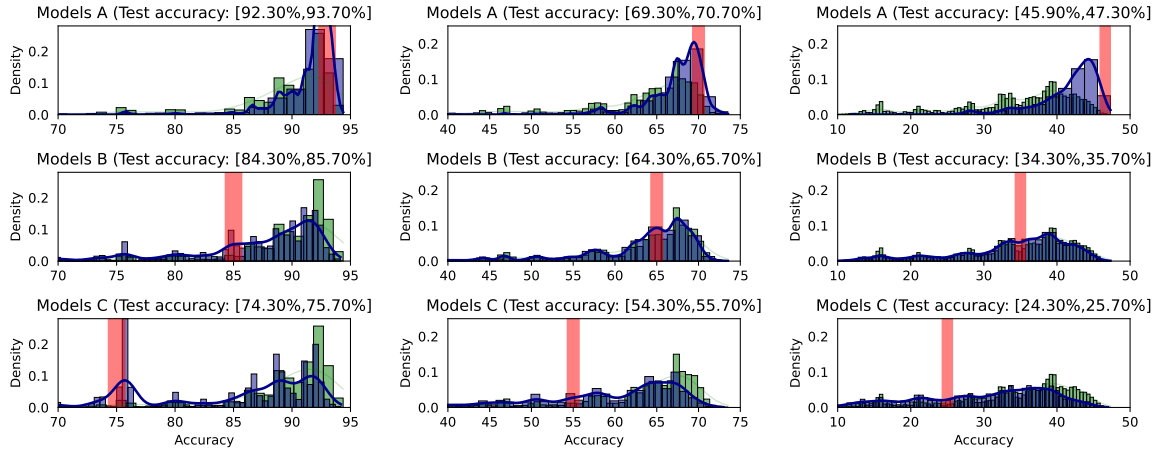


Figure 7: Histogram of test accuracies on radius-2 neighborhoods on NAS-Bench-201 on CIFAR-10 (left column); CIFAR-100 (middle column); ImageNet-16-120 (right column), for different reference architectures in the search space. The shaded red area refers to the range of test accuracies of the reference architectures, that is also reported in each subplot title. For each dataset, three accuracy ranges (corresponding to high, medium, and low performance) have been identified according to the difficulty of the dataset. The blue distribution regards the neighboring architectures. The green distribution regards the whole search space.

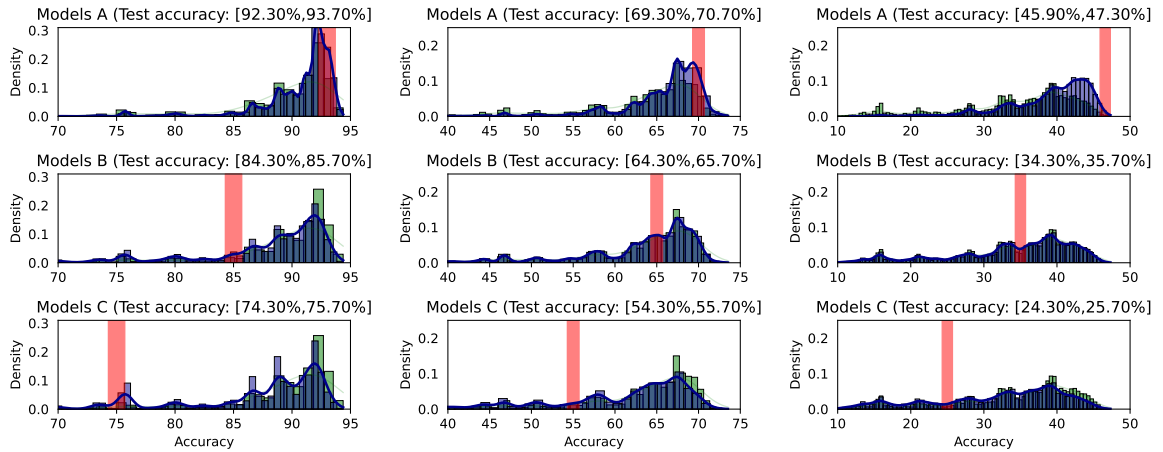


Figure 8: Histogram of test accuracies on radius-3 neighborhoods on NAS-Bench-201 on (left column) CIFAR-10; (middle column) CIFAR-100; (right column) ImageNet16-120, for different reference architectures in the search space. The red shaded area refers to the range of test accuracies of the reference architectures, that is also reported in each subplot title. For each dataset, three accuracy ranges (corresponding to high, medium, and low performance) have been identified according to the difficulty of the dataset. The blue distribution regards the neighboring architectures. The green distribution regards the whole search space.

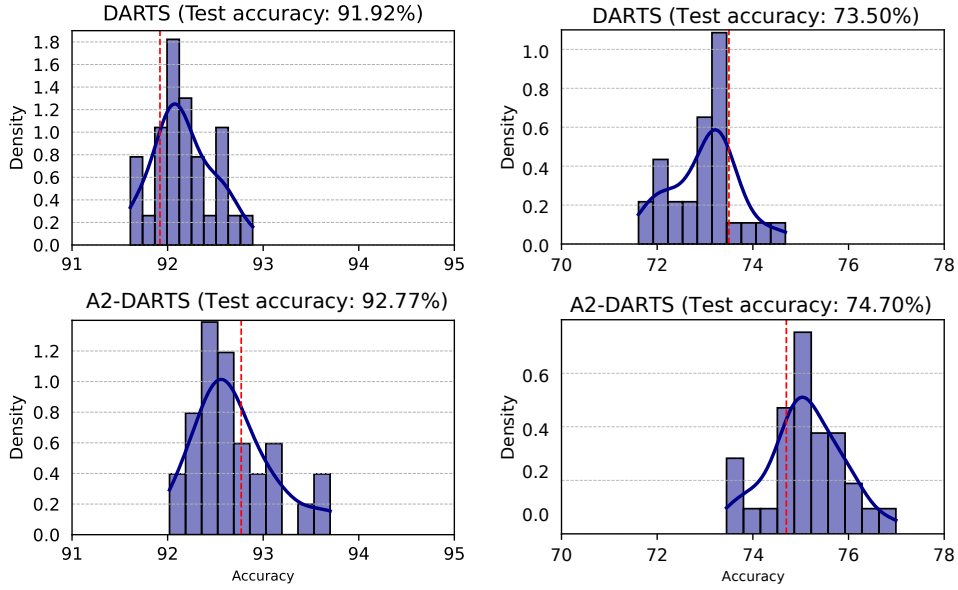


Figure 9: Histogram of test accuracies of radius-2 neighbors of a neural network architecture found by DARTS (upper panels) and A^2 -DARTS (lower panels) on CIFAR-10 (left column) and CIFAR-100 (right column). To obtain each histogram, 30 architectures have been sampled perturbing at random at radius 1 the initial configuration (whose accuracy is shown by the dashed red line), and trained until a fix loss threshold. We observe a local property around all initial architectures, with their neighbors taking accuracy values close to them. The highest accuracy networks cluster together, highlighting the presence of a flat region in neural architecture space extending even at radius 2.

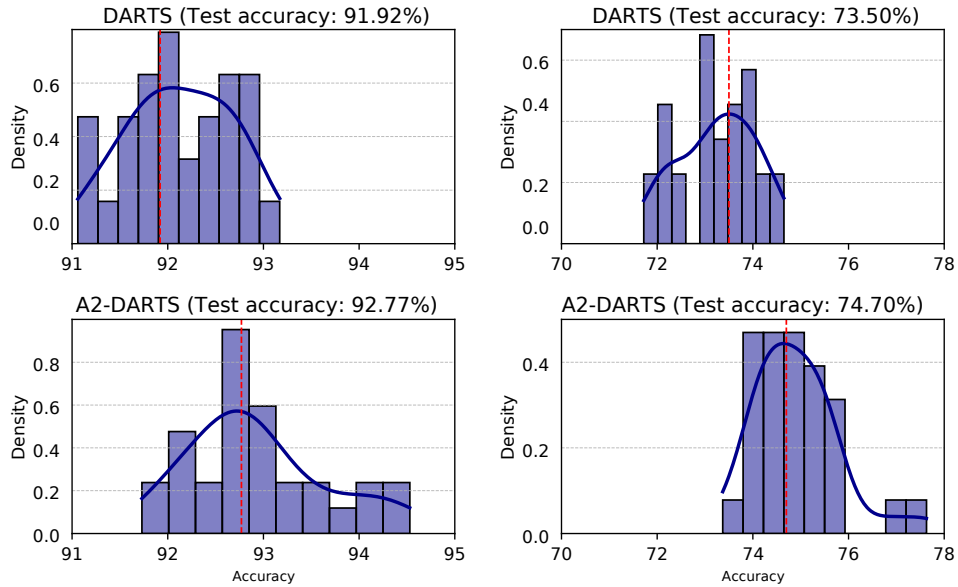


Figure 10: Histogram of test accuracies of radius-3 neighbors of a neural network architecture found by DARTS (upper panels) and A^2 -DARTS (lower panels) on CIFAR-10 (left column) and CIFAR-100 (right column). To obtain each histogram, 30 architectures have been sampled perturbing at random at radius 1 the initial configuration (whose accuracy is shown by the dashed red line), and trained until a fix loss threshold. We observe a local property around all initial architectures, with their neighbors taking accuracy values close to them. The highest accuracy networks cluster together, highlighting the presence of a flat region in neural architecture space extending even at radius 3.

C.2 Optimal ρ_α for A²M

In Fig. 11 we report the final model test accuracies varying ρ_α in the A²M algorithm on CIFAR-10. The best accuracies are achieved for $\rho_\alpha = 10^{-2}$ and $\rho_\alpha = 10^{-1}$ for NAS-Bench-201 and DARTS, respectively. We then use these values of ρ_α on all datasets.

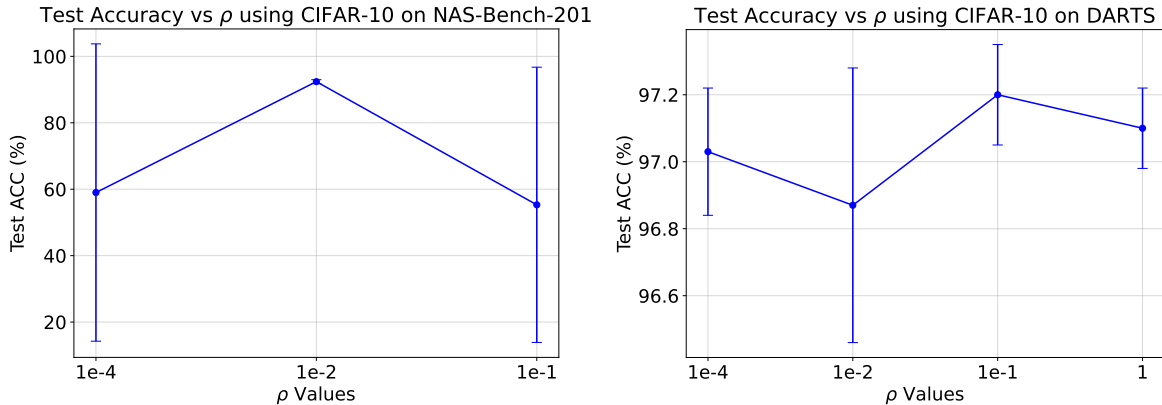


Figure 11: Test accuracies of the final NN models found on CIFAR-10 on the NAS-Bench-201 (left) and DARTS (right) search spaces by A²-DARTS in function of the hyperparameter ρ_α .

C.3 Validation accuracy on NAS-Bench-201

We report the accuracy of DARTS-based methods investigated in this paper on Nas-Bench-201 in Table 2.

Table 2: Validation accuracy on NAS-Bench-201 search space across CIFAR-10, CIFAR-100, and ImageNet16-120 datasets and several DARTS-based methods, showing standard and A²-enhanced results. *DARTS and A²-DARTS have been run without data augmentation on the valid set.

Model	CIFAR-10 Valid Acc (%)		CIFAR-100 Valid Acc (%)		ImageNet16-120 Valid Acc (%)	
	Standard	A ² -	Standard	A ² -	Standard	A ² -
DARTS (1st)* [6]	70.86 ± 34.09	89.64±0.65	49.42 ± 27.42	68.60±1.69	27.12 ± 15.58	41.96±1.86
β -DARTS [11]	91.40±0.18	91.40±0.18	72.70±1.0	72.70±1.0	45.97±0.37	45.97±0.37
Λ -DARTS [30]	89.75 ± 2.10	91.11±0.53	69.81 ± 3.54	72.00±1.72	43.18 ± 2.95	45.01±1.64
DARTS-PT[9]	85.30 ± 0.0	85.40±0.0	61.05 ± 0.0	63.28±0.0	35.18±0.0	33.63 ± 0.0
DARTS-[10]	90.20±0.47	90.20±0.47	70.71±1.60	70.71±1.60	40.78±1.58	40.78±1.58
SDARTS-RS[38]	75.21 ± 0.25	82.53±0.16	47.51 ± 0.39	54.53±0.31	27.79±0.68	27.45 ± 0.22
PC-DARTS[29]	68.28 ± 0.31	89.07±0.20	38.57 ± 0.88	66.43±0.46	18.87 ± 0.65	40.13±0.82
OPTIMAL [21]		91.61		73.49		45.56

C.4 Data Augmentation on the Validation Set of NAS-Bench-201

DARTS-based methods typically include data augmentation applied to the validation set. It is important to notice that architecture parameters in DARTS-based methods are trained using the validation set, meaning that augmentation can significantly influence search dynamics. Interestingly, as can be seen from Tables 1 and 2, we found that without data augmentation on NAS-Bench-201, standard DARTS does not suffer at every run of convergence to the degenerate architecture composed entirely of skip connections, although the issue remains present. This suggests a correlation between data augmentation and the DARTS instability towards degenerate solutions. In contrast, other DARTS-based methods generally benefit from data augmentation, likely because their regularization mechanisms are themselves able to mitigate the skip connection issue.

C.5 Implementing the β -DARTS regularization on the DARTS search space

The β -DARTS update rule has to be redefined to be compliant with the DARTS search space since this space contains two types of cells, i.e. normal and reduction ones [30]. We could not find, as of the beginning of March 2025, in the official β -DARTS repo <https://github.com/Sunshine-Ye/Beta-DARTS> scripts and code for directly running experiments with β -DARTS on the DARTS search space - in particular we could not find it in the `_backward_step` at line 80 of <https://github.com/Sunshine-Ye/Beta-DARTS/blob/master/optimizers/darts/architect.py>.

We therefore proceed to define the β -DARTS loss for the DARTS search space as:

$$\mathcal{L}_{\text{val}}(w, \alpha) + \lambda(w_{\text{nor}}\mathcal{L}_{\text{Beta}}(\alpha_{\text{nor}}) + w_{\text{red}}\mathcal{L}_{\text{Beta}}(\alpha_{\text{red}})) \quad (46)$$

with $\lambda = \text{epoch}/2$ as done in the original β -DARTS implementation. In our experiments we use the $\mathcal{L}_{\text{Beta}}$ regularization on both the architecture parameters of the normal and reduction cells, and we add the weights w_{nor} and w_{red} in the loss Eq. (46) to perform an additional hyperparameter tuning which is not reported in the original β -DARTS papers [11, 12]. To this aim we investigate how the hyperparameters w_{nor} and w_{red} impact the performance by applying more or less regularization to the normal or reduction cells. We report in Table 1 the best results on test accuracy we obtain for β -DARTS on each dataset by tuning these hyperparameters (which corresponds to $w_{\text{nor}} = 1.0$ and $w_{\text{red}} = 1.0$).

In Table 3 we show the test accuracy results obtained by β -DARTS on the DARTS search space and on CIFAR-10, CIFAR-100 and ImageNet-16-120, with different combinations of the w_{nor} and w_{red} weights, corresponding to: β -DARTS with equal importance on normal and reduction cells ($w_{\text{nor}} = 1.0$, $w_{\text{red}} = 1.0$), β -NOR with more importance on the normal cell ($w_{\text{nor}} = 1.6$, $w_{\text{red}} = 0.4$), β -RED with more importance on the reduction cell ($w_{\text{nor}} = 0.4$, $w_{\text{red}} = 1.6$).

Table 3: Final test accuracy of the models obtained by β -DARTS on the DARTS search space with different weights w_{nor} and w_{red} on the regularization of the normal and reduction cells. From top to bottom: (a) equal importance on normal and reduction cells ($w_{\text{nor}} = 1.0$, $w_{\text{red}} = 1.0$), (b) β -NOR with more importance on the normal cell ($w_{\text{nor}} = 1.6$, $w_{\text{red}} = 0.4$), (c) β -RED with more importance on the reduction cell ($w_{\text{nor}} = 0.4$, $w_{\text{red}} = 1.6$).

Model	CIFAR-10	CIFAR-100	ImageNet16-120
β -DARTS	96.83 \pm 0.15	81.85 \pm 0.68	53.92 \pm 0.47
β -NOR	96.82 \pm 0.30	81.49 \pm 1.00	48.47 \pm 0.53
β -RED	96.60 \pm 0.16	81.47 \pm 0.78	51.87 \pm 0.43